Journal of Materials Chemistry A

Accepted Manuscript

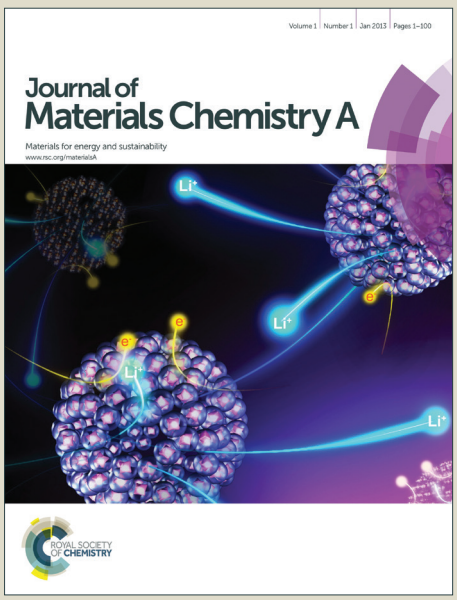

ROYAL SOCIETY OF CHEMISTRY

www.rsc.org/materialsA

Two Steps Reduction of Self-Assembly Three-Dimensional (3D) Reduced Graphene Oxide (RGO)/Zinc Oxide (ZnO) Nanocomposite for Electromagnetic Absorption

Fan Wu,[a‡]* *Yilu Xia,*[b‡] *Yuan Wang,*[a] *Mingyang Wang*[a]*

[a] State Key Laboratory for Disaster Prevention & Mitigation of Explosion & Impact, PLA University of Science and Technology, Nanjing 210007, P. R. China.

[b] School of Chemistry and Materials Science, Nanjing Normal University, Nanjing 210023, P. R. China.

ABSTRACT: Graphene oxide (GO) and zinc oxide (ZnO) nanoparticles has been formed a three-dimensional (3D) nanocomposite through hydrothermal process, and the further UV-irradiation remove the remained oxygen functional groups from the skeleton of reduced graphene oxide (RGO). This new type of 3D-RGO/ZnO nanocomposite exhibit a wide effective absorption bandwidth (deeper than − 10 dB) which was characterized as 6.4 GHz when filler loading is 10 wt% in composite and thickness of absorber is 2.5 mm. Therefore, combining the GO and ZnO nanoparticles into 3D nanocomposite can be considered as an effective route to design light weight and high performance electromagnetic absorption material.

1. INTRODUCTION

Recently, much attention has been focused on electromagnetic absorption materials, because electromagnetic pollution has harmful effects on electronic devices as well as on organisms. Electromagnetic interference (EMI) shielding materials are widely used in industrial, commercial and military fields, a good EMI shielding material should prevent both incoming and outgoing EMI,[1] thus electromagnetic absorption is more important than electromagnetic reflection during the development of this shielding material. An ideal electromagnetic absorption material should exhibit low density and thickness, strong absorption and broad bandwidth.[2] A number of nanomaterilas with specific morphology have been reported to absorb electromagnetic waves, including CuS,[3,4] Bi_2S_3,[5] intercalated graphite,[6] poly(3,4-ethylenedioxythiophene) (PEDOT),[7] α-MnO_2,[8,9] and ZnO nanorods.[10] Benefit with the nano-structure, a very low content ratio can reach an ideal electromagnetic absorption performance (less than 20 wt%).

Nowadays, remarkable progress has been made in self-assembly of nanomaterials into three-dimensional (3D) forms as hydrogels, aerogels, and some other micropores or mesopores frameworks.[11] Reduced graphene oxide (RGO) is a kind of two-dimensional (2D) carbon material which was synthesized from graphene oxide (GO) through chemical,[12] thermal,[13] optical,[14,15] and hydrothermal[16] methods. A great deal of work has shown the huge potential of RGO in various technological fields, such as polymer composites,[17-19] chemical and biological sensors,[20,21] energy-storage materials,[22-24] electrocatalysis,[25,26] and environmental protection materials.[27-29]

Dielectric loss and low density of RGO enable it to be used as an electromagnetic absorption material. With a suitable preparation process, pure RGO can display a good electromagnetic absorption performance.[30] The development of functional RGO modified with other nanoparticles also take an important advance to improve electromagnetic absorption, such as Fe_2O_3,[31,32] Fe_3O_4,[33,34] hematite,[35] Co_3O_4,[36] $MnFe_2O_4$,[37] polyaniline,[38,39] PEDOT,[40] and carbon nanotubes.[41] Furthermore, core-shell structure, for example, Fe_3O_4@ZnO,[42] SiO_2@Fe_3O_4,[43] and Fe_3O_4@Fe,[44] can also improve the absorption property.

In this work, we demonstrated the development of a new type of 3D-RGO/zinc oxide (ZnO) nanocomposite by a facile two-step reduction. First step of hydrothermal approach provide the 3D nanohybrid and remove most oxygen functional groups, and second step of UV catalysts reduction gives a chance to purify the RGO skeleton. Among a diverse range of semiconductor photocatalysts, ZnO nanoparticles have been considered as promising materials because of their low cost, relative nontoxicity, long-term thermodynamic stability and photostability, and unique semiconducting properties. Semiconductor nanomaterials have also been used in electromagnetic absorption field in recent years.[10,45] ZnO nanomaterials have been widely studied because of their excellent absorption properties.[10,46-48] It is worthy to point out that recent paper has reported that uniform ZnO nanorods through controllable synthesis can get an enhanced absorption properties with two peaks of reflection loss.[10] UV-assisted photocatalytic reduction of GO has been recognized,[14,15] and RGO/ZnO nanocomposite has received interesting in multi-application field, such as

dye-sensitized solar cells (DSSCs),[49] pollutant management,[50] electrochemical sensing.[51] However, the strategy of using RGO/ZnO nanocomposite for electromagnetic absorption has not been reported heretofore. Our findings showed that this new type RGO/ZnO nanocomposite with 3D interconnected networks can greatly improve the electromagnetic absorption performance. Furthermore, benefit from the second step of UV reduction, effective absorption bandwidth and maximum absorption value, which are two important targets in electromagnetic absorption can be further improved. These unique properties shows 3D-RGO/ZnO nanocomposite is able to become an ideal electromagnetic absorption material with low adjunction (10 wt%), tiny thickness (2.0-3.0 mm), strong absorption (− 25 dB) and broad effective absorption bandwidth (6.40 GHz) simultaneously.

2. EXPERIMENTAL SECTION

2.1. Materials. Graphite powder (200 mesh, 99.9999%) was purchased from Alfa Aesar Co., Ltd, United States. Zinc oxide (ZnO) nanoparticles was purchased from Aladdin Industrial Inc., Shanghai, China. Ethanol (99.5%) was purchased from GENERAL-REAGENT, Titan Scientific Co., Ltd, Shanghai, China. Concentrated sulfuric acid (H_2SO_4, 98%), potassium permanganate ($KMnO_4$), hydrogen peroxide (H_2O_2, 30%), hydrochloric acid (HCl, 38%) were given by Prof. W. Dong, Nanjing University of Science & Technology, China. Distilled water was obtained from Direct-Q3 UV, Millipore.

2.2. Synthesis and Purification of Graphene Oxide (GO). Graphite oxide was

synthesized by a modified Hummers method firstly. In brief, 2.0 g of graphite was first mixed in a solution of 100.0 ml of H_2SO_4 in an ice bath for 3 hours. Then, 8.0 g of $KMnO_4$ was slowly added into the solution. After it was stirred for 2 hours, 200.0 mL of distilled water was added drop by drop under ordinary temperature water bath. After additional 30 minutes stirring, 10.0 mL of H_2O_2 was slowly added into the above-mentioned solution, and a bright yellow of graphite oxide appearance during this process. The graphite oxide was filtered and washed by distilled water for 4 times to remove all the impurity. Then, the gel like graphite oxide was freezed-dried at −50 °C for 24 hours to obtain graphite oxide powder. The graphite oxide powder was dispersed in distilled water as 1 mg mL^{-1}, and centrifuged at 10000 rap min^{-1} for 30 minutes to remove all the agglomerate sheets. And the GO was obtained at supernatant and dried at 50 °C.

2.3. Synthesis of Two Steps Reduction 3D-RGO/ZnO Nanocomposite. 60.0 mg of GO was dispersed in 20.0 mL of distilled water by sonication for 30 minutes. ZnO nanoparticles was also dispersed in 40 mL of distilled water through intensive sonication. Two nanocomposites with the weight ratios of the raw material as GO to ZnO nanoparticles, 4 : 1 (sample-1) and 1 : 1 (sample-2). Then, ZnO dispersion was added into GO dispersion drop by drop. These hybrids solution was stirred with high speed for 1 hour. After that, the above mentioned solution was sealed in a 100-mL Teflon-lined autoclave and maintained at 180 °C for 12 hours. Then the autoclave was naturally cooled to room temperature and the as-prepared 3D-RGO/ZnO was taken out and subsequently freezed-dried for 24 hours to obtain 3D-RGO/ZnO. This

nanocomposite was grinded into powder and then put into ethanol solution. UV-irradiation was performed by an UV-light curing system (UV-1318, Zhuhai Kaivo Optoelectronic Technology Co., Ltd., China) with a 250 W high pressure mercury lamp for 4 hours. A mini-fan, which was assisted in maintaining the temperature (30 $^{\circ}$C) during irradiation with minimum variation in the experimental results. Finally, the sample was filtered out and dried at 30 $^{\circ}$C under vacuum. This synthesis process has been summarized in scheme 1.

2.4. Characterization and Measurement. Energy dispersive X-ray (EDX) analysis was carried out in environment scanning electron microscope (ESEM, XL-30, Philips). The detailed morphologies of the 3D-RGO, 3D-RGO/ZnO were observed with a field emission scanning electron microscope (FE-SEM, S4800, Hitachi) and field emission high resolution transmission electron microscope (FE-HRTEM, Tecnai G2 F30 S, FEI). The crystal structure of the as-synthesized samples was identified by X-ray diffractometer (XRD, X' Pert Pro, Philips), using Cu Kα (λ = 1.54 Å) radiation. X-ray photoelectron spectra (XPS) was carried out in a Thermo Scientific ESCALAB 250Xi X-ray photoelectron spectrometer equipped with a monochromatic Al Kα X-ray source (1486.6 eV).

2.5. Dielectric and Electromagnetic Absorption Property Characterization. The relative complex permittivity (ε_r) and permeability (μ_r) were measured by a vector network analyzer (VNA, N5242A PNA-X, Agilent) in the frequency range of 2-18 GHz. The measured samples were prepared by uniformly mixing 10.0 wt% of 3D-RGO/ZnO with a paraffin matrix at 100 °C. The mixture was then pressed into

toroidal shaped samples with an outer diameter of 7.00 mm and inner diameter of 3.04 mm. In a coaxial wire analysis, ε_r of the dielectric material has been calculated from the experimental scattering parameters S_{11} (or S_{22}) and S_{21} (or S_{12}) using the standard Nicolson-Ross-Weir (NRW) algorithm.[52,53]

Due to the frequency range is from 2-18 GHz, the source-to-shield distance be greater than the free-space wavelength, so the measurements are considered under far field.[54] According to the transmission line theory,[55] the input impedance (Z_{in}) on the interface can be expressed as

$$Z_{in} = Z_0\sqrt{\frac{\mu_r}{\varepsilon_r}}tanh\left(j\frac{2\pi fd}{c}\sqrt{\varepsilon_r\mu_r}\right) \quad (1)$$

Where Z_0 is the impedance of free space, μ_r is the complex permeability, $\mu_r = \mu' - j\mu''$, ε_r is the complex permittivity, $\varepsilon_r = \varepsilon' - j\varepsilon''$, f is the frequency, d is the thickness of material, c is the speed of light.

On the basis of the model of metal backplane, the reflection loss (RL) of a sample is determined from Z_0 and Z_{in} according to the following equation

$$\mathrm{RL(dB)} = 20\lg\left|\frac{Z_{in}-Z_0}{Z_{in}+Z_0}\right| \quad (2)$$

When the RL is lower than – 10 dB, 90% of the electromagnetic energy is absorbed.

3. RESULTS AND DISCUSSION

GO nanosheets which attached ZnO nanoparticles on their surface formed a 3D nanocomposite during the hydrothermal process, and GO was reduced to RGO. The diffraction peak of graphite (002) in Figure 1 illustrate that the most oxygen functional groups has been removed from GO's surface.[16] The strong and quite sharp

diffraction peaks observed at 2θ = 31.78, 34.42, 36.26, 47.52, 56.60° reveal highly close to the standard XRD data for the (100), (002), (101), (102) and (110) planes of ZnO. The intensity of XRD in sample-2 is much higher than sample-1 can attribute to the high ZnO containing ratio.

Figure 2a shows the ESEM image of 3D-RGO/ZnO nanocomposite, from it, this nanocomposite has an interconnected 3D porous network with submicrometer and micrometer pores. In order to know the dispersion of ZnO nanoparticles in this 3D nanocomposite, EDX mapping analysis of C, O, and Zn (Figure 2b-d) was used and we clearly verified the ZnO nanoparticles throughout the 3D macroporous structure. Figure 2e and f shows the detail morphologies of 3D-RGO/ZnO under FE-SEM, ZnO nanoparticles can clearly find on the RGO skeleton surface. FE-HRTEM was used to investigate the crystal size of morphology of ZnO nanoparticles. Figure 2g shows the FE-HRTEM of pure 3D-RGO. In Figure 2h shows that the nanoparticles of ZnO with a size of about 150-200 nm are symmetrically attached onto the RGO's surface, and no ZnO nanoparticles are disassociated from the RGO's surface were observed.

The C 1s XPS spectrum of GO and 3D-RGO/ZnO nanocomposite through two steps reduction has been shown in Figure 3. There are four types of carbon bonds, include C–C (284.8 eV), C–O (286.6 eV), C=O (288.0 eV), and O–C=O (289.2 eV), indicate that GO has been highly oxidized (Figure 4a). Although the C 1s XPS spectra of 1st reduction 3D-RGO/ZnO (Figure 4b) also has the oxygenated groups, but they are much weaker then GO. After UV-irradiation, C=O and O–C=O structure are hardly found from Figure 4c, it can imply that these structures have been reduced by

the emission quenching represents electron transfer from the excited ZnO nanoparticles to the RGO skeleton.[15] Combining with this result and considering with the Lerf-Klinowski model of GO,[56,57] carboxyl was at the edge of GO's platelet, therefor, second reduction rebuilt the honeycomb structure at the edge. In order to realize diversification of oxygen groups on RGO's surface, HCl was used to etch ZnO nanoparticles and the C/O ratio of the remained 3D-RGO was characterized by XPS after washing, filtrating and evaporation. In Table 1, the C/O ratio clearly shows that oxygen groups are replaced gradually through two steps reduction.

The permittivity of each samples was measured by coaxial wire method.[52] Figure 4 shows the ε′ and ε″ measured in the frequency range of 2-18 GHz for each samples before and after UV-irradiation. As shown in Figure 4a, c, the values of ε′ decrease with increasing frequency in both samples, no matter before and after UV-irradiation. Furthermore, when the weight ratio of ZnO was improved, the values of ε′ also decrease in the whole frequency range (blue line in Figure 4a, c). After UV-irradiation, the values of ε″ keep stable relatively, meanwhile, the values of ε″ of first step reduction 3D-RGO/ZnO decrease with increasing frequency obviously. Due to ε″ is a measure of dielectric losses, it is easy to accept that large ε″ should bring strong electromagnetic absorption. However, in a composite filled with dielectric particles only, at the best matching condition, the maximum RL as follows:[58]

$$RL_{max} = 20\lg\left|\frac{\frac{1}{\varepsilon}-1}{\frac{1}{\varepsilon}+1}\right| \quad (3)$$

after some transformation, we obtain

$$RL_{max} = 20\lg\left(1 - \frac{4}{2+\varepsilon''\left(tan\delta+\frac{1}{tan\delta}\right)}\right) \quad (4)$$

thus, maximum RL should be evaluated by considering both ε″ and dielectric loss tangent (tanδ). This is further confirmed by the attenuation constant (α),[58]

$$\alpha = \frac{\omega}{\sqrt{2c}}\sqrt{-\varepsilon' + \sqrt{(\varepsilon'^2 + \varepsilon''^2)}} \quad (5)$$

after some transformation and matching frequency, α reads as,

$$\alpha = \frac{\omega}{\sqrt{2d}}\sqrt{\frac{1}{\varepsilon''}\left(\sqrt{1+\frac{1}{tan^2\delta}} - \frac{1}{tan\delta}\right)} \quad (6)$$

In Figure 5 and Figure 6, tanδ and α has been shown respectively. The tanδ = ε″/ε′, where δ is the dielectric loss angle of the material. Energy loss in a material illuminated by electromagnetic waves comes about through damping forces acting on polarized atoms and molecules and through the finite conductivity of a material. Due to the contribution of large ε″ in the first step hydrothermal reduction of 3D-RGO/ZnO, they have much larger values of tanδ than these samples after UV-irradiation. However, after calculated through the formula of α, 3D-RGO/ZnO which go through two steps reduction, has lager attenuation constant in the whole frequency range. It imply that these samples should have better electromagnetic absorption performance, and also explain that too large ε″ will not be in favor of absorption.

RL values of composite at various thickness can be obtained through formula (1) and (2). Figure 7 shows the RL curves of sample-1 and sample-2 at different thickness (2.0, 2.5, and 3.0 mm) in the frequency range 2-18 GHz with a filler loading of 10.0 wt%. It is obviously found that electromagnetic absorption performance has been

enhanced after UV-irradiation. Before UV-irradiation, compared with sample-1 and sample-2, the latter has better electromagnetic absorption performance profit from high loading ratio of ZnO nanoparticles, which has pretty good electrical conductivity and dielectric loss. Table 2 has been given the key data of electromagnetic absorption. In sample-1, before UV-irradiation, only with the thickness of 2.0 mm, it has a very week and narrow effective absorption bandwidth. But after UV-irradiation, a significant absorption peak has been appeared, for 2.0, 2.5, and 3.0 mm thickness, effective absorption bandwidth increase from 1.84 to 5.08, 0 to 6.16, 0 to 4.68 GHz. Meanwhile, the maximum RL values also increase from – 10.53 to – 23.12, – 8.67 to – 20.92, – 7.92 to – 25.95 dB, respectively. In sample-2, due to high loading ratio (100 wt% to GO) of ZnO nanoparticles, it has an apparent absorption peak before UV-irradiation. After UV-irradiation process, this performance has been enhanced further, it can be characterized as effective absorption bandwidth increase from 2.84 to 2.92, 6.24 to 6.40, 5.16 to 5.76 GHz, and the maximum RL values increase from – 20.27 to – 25.31, – 19.88 to – 24.84, – 19.35 to – 25.31 dB respectively during the thickness increase from 2.0 to 3.0 mm. These results imply that this material has the main requirements for the dielectric based electromagnetic absorbers such as (i) it should increase the absorption of electromagnetic waves through high values of dielectric and magnetic losses; (ii) it is expected to be applied in a wide frequency range (6.4 GHz for maximum effective absorption bandwidth); (iii) it has a low loading in composites (10 wt% in this work); and (iv) it does not require the use of an external magnetic field.[3-10,38-41,58]

We consider that Debye dipolar relaxation is an important mechanism by which dielectric absorption materials absorb electromagnetic radiation. The relative complex permittivity can be expressed by the following equation:[3,6]

$$\varepsilon_r = \varepsilon_\infty + \frac{\varepsilon_s - \varepsilon_\infty}{1 + j2\pi f\tau} \quad (7)$$

Where f, ε_s, ε_∞, and τ are the frequency, static permittivity, relative dielectric permittivity at the high-frequency limit, and polarization relaxation time, respectively. Thus, ε' and ε'' can be described by

$$\varepsilon' = \varepsilon_\infty + \frac{\varepsilon_s - \varepsilon_\infty}{1 + (2\pi f)^2\tau^2} \quad (8)$$

$$\varepsilon'' = \frac{2\pi f\tau(\varepsilon_s - \varepsilon_\infty)}{1 + (2\pi f)^2\tau^2} \quad (9)$$

According to (8) and (9), the relationship between ε' and ε'' can be expressed:

$$(\varepsilon' - \frac{\varepsilon_s - \varepsilon_\infty}{2})^2 + (\varepsilon'')^2 = (\frac{\varepsilon_s - \varepsilon_\infty}{2})^2 \quad (10)$$

Thus, the plot of ε' versus ε'' would be a single semicircle, generally denoted as the Cole-Cole semicircle. Each semicircle corresponds to one Debye relaxation process. Figure 8 shows the ε'-ε'' curves of sample 1 and 2 before and after UV-irradiation. No obvious conspicuous semicircles have been found before UV-irradiation. On the contrary, UV-reduction gives rise to interfacial polarization or Maxwell-Wagner effect, and the several semicircles in each curve (Figure 8c and 8d) imply that other kinds of relaxation, such as Maxwell-Wagner relaxation and electron polarization.[3,6,59,60]

4. CONCLUSION

3D-RGO/ZnO nanocomposite were prepared via two steps reduction. ZnO nanoparticles attached on GO's surface and were assembled a 3D hydrogel through the first step of hydrothermal reduction. Electromagnetic absorption performance has

been enhanced after the second reduction through UV-irradiation. The maximum effective absorption bandwidth could reach 6.4 GHz when filler loading is 10 wt% in composite and thickness of absorber is 2.5 mm. This work provides a facile method to fabricate a potential and excellent electromagnetic absorption material with low loading ratio and wide absorption bandwidth.

Corresponding Author

E-mail addresses: wufanjlg@163.com (F. Wu).

E-mail addresses: wmyrf@163.com (M. Y. Wang), Tel.: +86 25 80825361.

Author Contributions

‡These authors contributed equally.

ACKNOWLEDGMENT

This work was financially supported by the National Natural Science Foundation of China (51403236, 51021001) and the Opening Project of State Key Laboratory of Disaster Prevention & Mitigation of Explosion & Impact (DPMEIKF201310).

REFERENCES

1 H. R. Tantawy, D. E. Aston, J. R. Smith and J. L. Young, *ACS Appl. Mater. Interfaces*, 2013, **5**, 4648.

2 Z. Chen, C. Xu, C. Ma, W. Ren and H. M. Cheng, *Adv. Mater.*, 2013, **25**, 1296.

3 S. He, G. S. Wang, C. Lu, J. Liu, B. Wen, H. Liu, L. Guo and M. S. Cao, *J. Mater. Chem. A*, 2013, **1**, 4685.

4 Y. Z. Wei, G. S. Wang, Y. Wu, Y. H. Yue, J. T. Wu, C. Lu and L. Guo, *J. Mater. Chem. A*, 2014, **2**, 5516.

5 X. Luo, G. S. Wang, H. Y. Guo, X. J. Zhang, W. Q. Cao, Y. Z. Wei, L. Guo and M. S. Cao, *ChemPlusChem*, 2014, **79**, 1089.

6 G. S. Wang, X. J. Zhang, Y. Z. Wei, S. He, L. Guo and M. S. Cao, *J. Mater. Chem. A*, 2013, **1**, 7031.

7 F. Wu, Z. H. Xu, Y. Wang and M. Y. Wang, RSC Adv., 2014, 4, 38797.

8 M. Zhou, X. Zhang, J. M. Wei, S. L. Zhao, L. Wang and B. X. Feng, *J. Phys. Chem. C*, 2011, **115**, 1398.

9 G. S. Wang, S. He, X. Luo, B. Wen, M. M. Lu, L. Guo and M. S. Cao, *RSC Adv.*, 2013, **3**, 18009.

10 G. S. Wang, Y. Y. Wu, X. J. Zhang, Y. Li, L. Guo and M. S. Cao, *J. Mater. Chem. A*, 2014, **2**, 8644.

11 Y. Gao and Z. Tang, *Small*, 2011, **7**, 2133.

12 D. Li, M. B. Müller, S. Gilje, R. B. Kaner and G. G. Wallace, *Nat. Nanotech.*, 2008, **3**, 101.

13 C. D. Zangmeister, *Chem. Mater.*, 2010, **22**, 5625.

14 G. Williams, B. Seger and P. V. Kamat, *ACS Nano*, 2008, **2**, 1487.

15 G. Williams and P. V. Kamat, *Langmuir*, 2009, **25**, 13869.

16 Y. Xu, K. Sheng, C. Li and G. Shi, *ACS Nano*, 2010, **4**, 4324.

17 S. Stankovich, D. A. Dikin, D. H. B. Dommett, K. M. Kohlhaas, E. J. Zimney, E. A. Stach, R. D. Piner, S. T. Nguyen and R. S. Ruoff, *Nature*, 2006, **442**, 282.

18 T. Ramanathan, A. A. Abdala, S. Stankovich, D. A. Dikin, M. Herrera-Alonso, R. D. Piner, D. H. Adamson, H. C. Schniepp, X. Chen, R. S. Ruoff, S. T. Nguyen, I. A. Aksay, R. K. Prud'homne and L. C. Brinson, *Nat. Nanotech.*, 2008, **3**, 327.

19 J. Liang, Y. Huang, L. Zhang, Y. Wang, Y. Ma, T. Guo and Y. Chen, *Adv. Funct. Mater.*, 2009, **19**, 2297.

20 L. Zhang, G. Chen, M. N. Hedhili, H. Zhang and P. Wang, *Nanoscale*, 2012, **4**, 7038.

21 M. Liu, J. Song, S. Shuang, C. Dong, J. D. Brennan and Y. A. Li, *ACS Nano*, 2014, **8**, 5564.

22 C. Liu, Z. Yu, D. Neff, A. Zhamu and B. Z. Jang, *Nano Lett.*, 2010, **10**, 4863.

23 W. Gao, N. Singh, L. Song, Z. Liu, A. L. M. Reddy, L. Ci, R. Vajtai, Q. Zhang, B. Wei and P. M. Ajayan, *Nat. Nanotech.*, 2011, **6**, 496.

24 M. F. El-kady, V. Strong, S. Dubin and R. B. Kaner, *Science*, 2012, **335**, 1326.

25 V. Tjioa, J. Chua, S. S. Pramana, J. Wei, S. G. Mhaisalkar and N. Mathews, *ACS Appl. Mater. Interfaces*, 2012, **4**, 3447.

26 F. Gong, Z. Li, H. Wang and Z. S. Wang, *J. Mater. Chem.*, 2012, **22**, 17321.

27 H. Bi, X. Xie, K. Yin, Y. Zhou, S. Wan, L. He, F. Xu, F. Banhart, L. Sun and R. S. Ruoff, *Adv. Fucnt. Mater.*, 2012, **22**, 4421.

28 Y. He, Y. Liu, T. Wu, J. Ma, X. Wang, Q. Gong, W. Kong, F. Xing, Y. Liu and J. Gao, *J. Hazard. Mater.*, 2013, **260**, 796.

29 D. Wang, H. Gao, E. Roze, K. Qu, W. Liu, Y. Shao, S. Xin and Y. Wang, *J. Mater. Chem. C*, 2013, **1**, 5772.

30 X. J. Zhang, G. S. Wang, W. Q. Cao, Y. Z. Wei, M. S. Cao and L. Guo, *RSC Adv.*, 2014, **4**, 19594.

31 L. Kong, X. W. Yin, Y. J. Zhang, X. Y. Yuan, Q. Li, F. Ye, L. F. Cheng and L. T. Zhang, *J. Phys. Chem. C*, 2013, **117**, 19701.

32 H. Zhang, A. J. Xie, C. P. Wang, H. S. Wang, Y. H. Shen and X. Y. Tian, *J. Mater. Chem. A*, 2013, **1**, 8547.

33 C. G. Hu, Z. Y. Mou, G. W. Lu, N. Chen, Z. L. Dong, M. J. Hu and L .T. Qu, *Phys. Chem. Chem. Phys.*, 2013, **15**, 13038.

34 Y. L. Ren, C. L. Zhu, S. Zhang, C. Y. Li, Y. J. Chen, P. Gao, P. P. Yang and Q. Y. Ouyang, *Nanoscale*, 2013, **5**, 12296.

35 D. Chen, G. S. Wang, S. He, J. Liu, L. Guo and M. S. Cao, *J. Mater. Chem. A*, 2013, **1**, 5996.

36 P. B. Liu, Y. Huang and X. Sun, *ACS Appl. Mater. Interfaces*, 2013, **5**, 12355.

37 X. J. Zhang, G. S. Wang, W. Q. Cao, Y. Z. Wei, J. F. Liang, L. Guo and M. S. Cao, *ACS Appl. Mater. Interfaces*, 2014, **6**, 7471.

38 K. Singh, A. Ohlan, V. H. Pham, R. Balasubramanjyan, S. Varshney, J. Jang, S. H. Hur, W. M. Choi, M. Kumar, S. K. Dhawan, B. S. Kong and J. S. Chung, *Nanoscale*, 2013, **5**, 2411.

39 X. Chen, F. Meng, Z. Zhou, X. Tian, L. Shan, S. Zhu, X. Xu, M. Jiang, L. Wang, D. Hui, Y. Wang, J. Lu and J. Gou, *Nanoscale*, 2014, **6**, 8140.

40 F. Wu, Y. Wang and M. Y. Wang, *RSC Adv.*, 2014, **4**, 49780.

41 L. Kong, X. W. Yin, X. Y. Yuan, Y. J. Zhang, X. M. Liu, L. F. Cheng and L. T. Zhang, *Carbon*, 2014, **73**, 185.

42 D. Sun, Q. Zou, Y. Wang, Y. Wang, W. Jiang and F. Li, *Nanoscale*, 2014, **6**, 6557.

43 Y. Ren, C. Zhu, S. Zhang, C. Li, Y. Chen, P. Gao, P. Yang and Q. Y. Ouyang, *Nanoscale*, 2013, **5**, 12296.

44 Y. L. Ren, H. Y. Wu, M. M. Lu, C. L. Zhu, P. Gao, M. S. Cao, C. Y. Li and Q. Y. Ouyang, *ACS Appl. Mater. Interfaces*, 2012, **4**, 6436.

45 G. Wang, Z. Gao, S. Tang, C. Chen, F. Duan, S. Zhao, S. Lin, Y. Feng, L. Zhou and Y. Qin, *ACS Nano*, 2012, **6**, 11009.

46 Y. Chen, M. Cao, T. Wang and Q. Wan, *Appl. Phys. Lett.*, 2004, **84**, 3367.

47 M. S. Cao, X. L. Shi, X. Y. Fang, H. B. Jin, Z. L. Hou, W. Zhou and Y. J. Chen, *Appl. Phys. Lett.*, 2007, **91**, 203110.

48 H. B. Lin, M. S. Cao, Q. L. Zhao, X. L. Shi, D. W. Wang and F. C. Wang, *Scr. Mater.*, 2008, **59**, 780.

49 F. Xu, J. Chen, X. Wu, Y. Zhang, Y. Wang, J. Sun, H. Bi, W. Lei, Y. Ni and L. Sun, *J. Phys. Chem. C*, 2013, **117**, 8619.

50 J. Wang, T. Tsuzuki, B. Tang, X. Hou, L. Sun and X. Wang, *ACS Appl. Mater. Interfaces*, 2012, **4**, 3084.

51 P. Nayak, B. Anbarasan and S. Pamaprabhu, *J. Phys. Chem. C*, 2013, **117**, 13202.

52 A. M. Nicolson and G. F. Ross, *IEEE Trans. Instrum. Meas.*, 1970, **4**, 377.

53 W. B. Weir, *Proc. IEEE*, 1974, **62**, 33.

54 N. F. Colaneri and L. W. Shacklette, *IEEE Trans. Instrum. Meas.*, 1992, **41**, 291.

55 Y. Naito and K. Suetake, *IEEE Tran. Microwave Theory*, 1971, **19**, 65.

56 A. Lerf, H. He, M. Forster and J. Klinowski, *J. Phys. Chem. B*, 1998, **102**, 4477.

57 H. He, J. Klinowski, M. Forster and A. Lerf, *Chem. Phys. Lett.*, 1998, **287**, 53.

58 F. Qin and C. Brosseau, *J. Appl. Phys.*, 2012, **111**, 061301.

59 B. Wen, M. S. Cao, Z. L. Hou, W. L. Song, L. Zhang, M. M. Lu, H. B. Jin, X. Y. Fang, W. Z. Wang and J. Yuan, *Carbon*, 2013, **65**, 124.

60 M. M. Lu, W. Q. Cao, H. L. Shi, X. Y. Fang, J. Yang, Z. L. Hou, H. B. Jin, W. Z. Wang, J. Yuan and M. S. Cao, *J. Mater. Chem. A*, 2014, **2**, 10540.

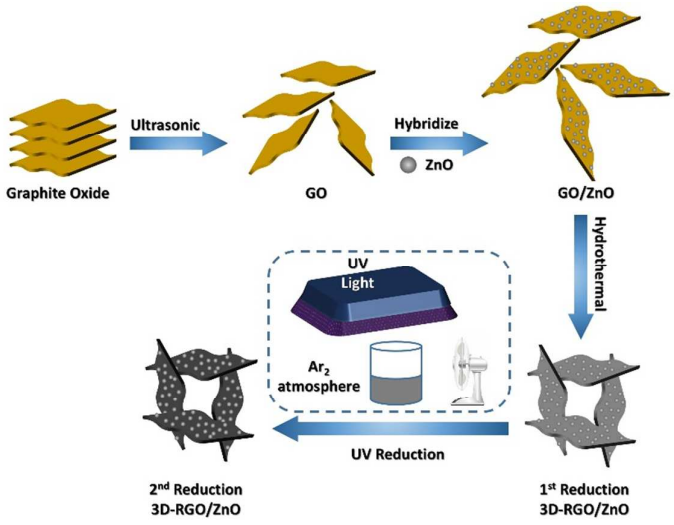

Scheme 1. Synthesis strategy for two steps reduction 3D-RGO/ZnO.

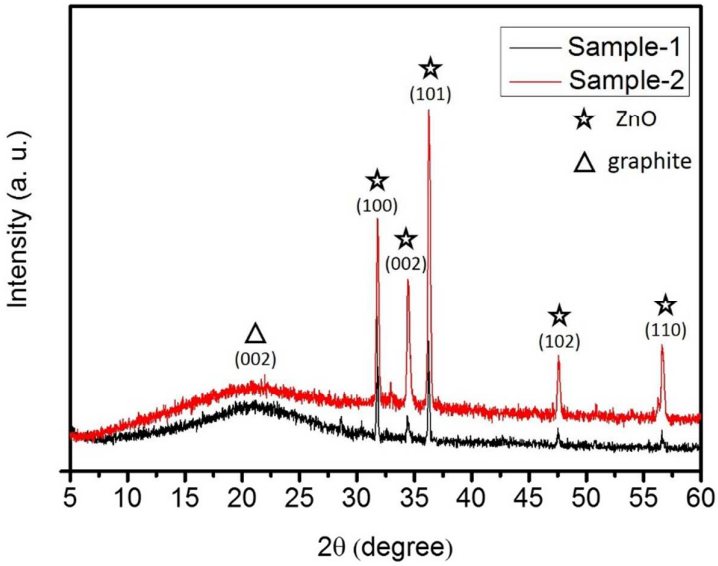

Figure 1. XRD spectra of hydrothermal reduction 3D-RGO/ZnO.

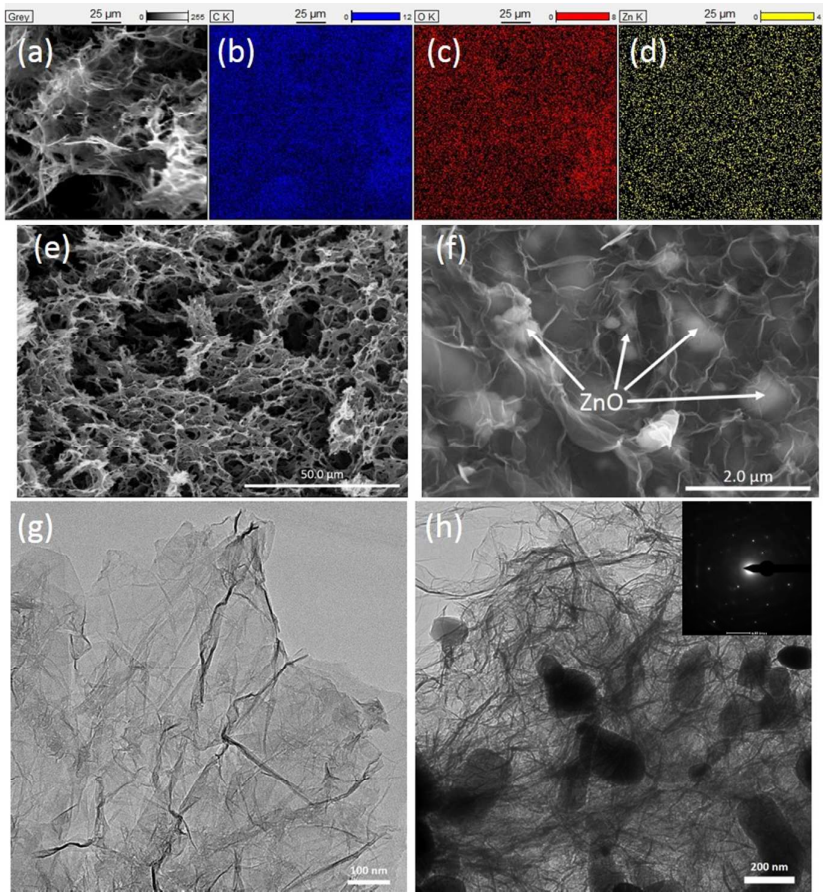

Figure 2. ESEM image of 3D-RGO/ZnO (a); EDX mapping of C (b), O (c), Zn (d) elements of (a); FE-SEM images of 3D-RGO/ZnO (e, f); FE-HRTEM images of 3D-RGO (g) and 3D-RGO/ZnO (h).

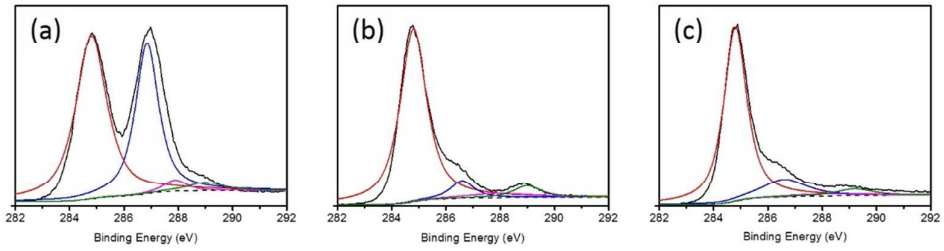

Figure 3. The C 1s XPS spectra of (a) GO, (b) 1st reduction 3D-RGO/ZnO and (c) 2nd reduction 3D-RGO/ZnO.

Table 1. C/O ratio of sample-1 and sample-2 characterized by XPS.

		GO	1st reduction	2nd reduction
C/O ratio	Sample-1	2.32	5.88	6.35
	Sample-2		5.86	6.93

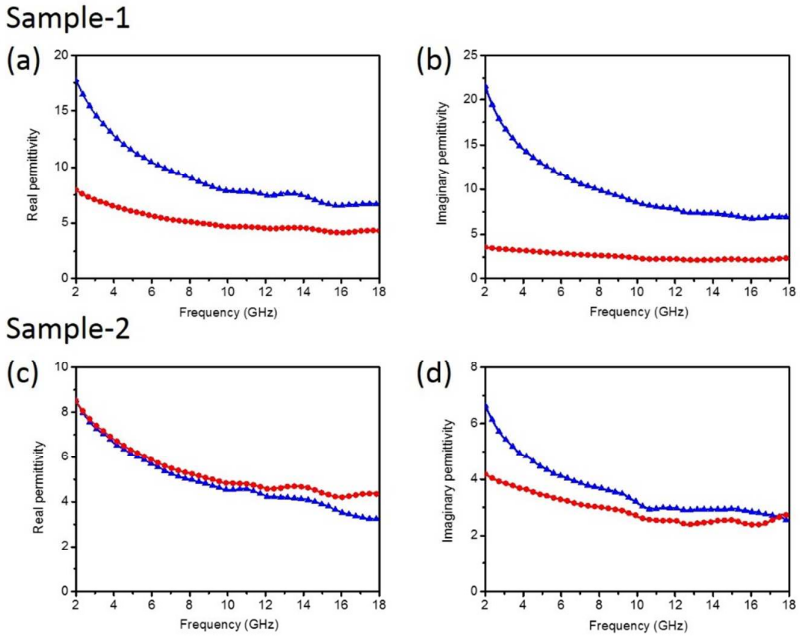

Figure 4. Real part (a) and imaginary part (b) of relative complex permittivity of sample-1 before (blue) and after (red) UV- irradiation; real part (c) and imaginary part (d) of relative complex permittivity of sample-2 before (blue) and after (red) UV-irradiation.

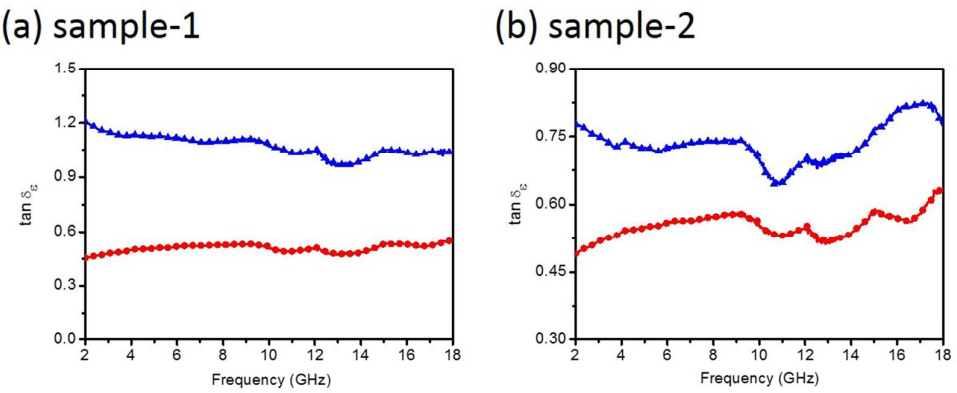

Figure 5. Dielectric loss tangent of sample-1 (a) and sample-2 (b) before (blue) and after (red) UV-irradiation in the frequency range of 2-18 GHz.

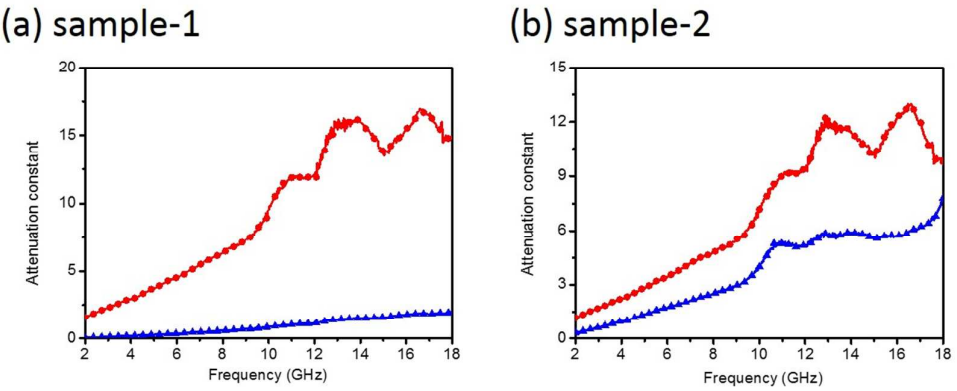

Figure 6. Attenuation constant of sample-1 (a) and sample-2 (b) before (blue) and after (red) UV-irradiation in the frequency range of 2-18 GHz.

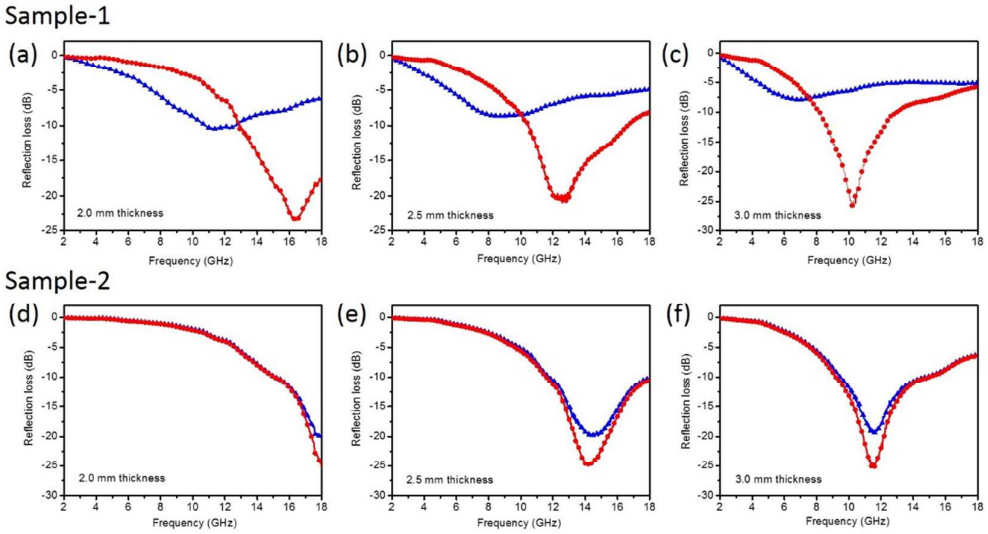

Figure 7. Reflection loss curves of sample-1 (a, b, c) and sample-2 (d, e, f) with the thickness of 2.0, 2.5 and 3.0 mm in the frequency range of 2-18 GHz before (blue) and after (red) UV-irradiation.

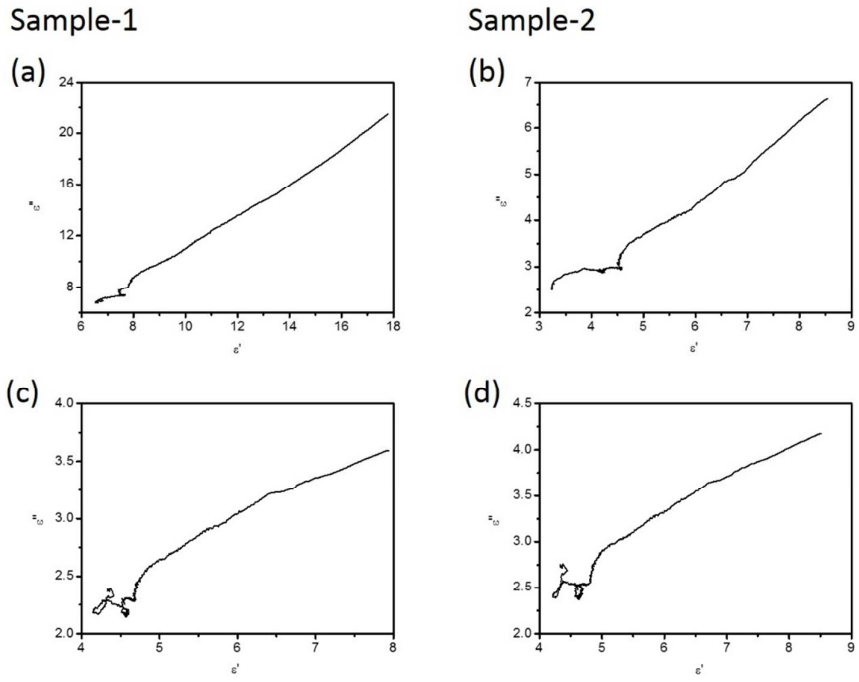

Figure 8. ε′-ε″ curves of 3D-RGO/ZnO before (a, b) and after (c, d) UV-irradiation.

Table 2. Electromagnetic absorption performance of sample-1 and sample-2 in different thickness before and after UV-irradiation.

Thickness (mm)		Maximum RL (dB)		Maximun RL position (GHz)		Effective absorption bandwidth (GHz)	
		Before UV-irradiation	After UV-irradiation	Before UV-irradiation	After UV-irradiation	Before UV-irradiation	After UV-irradiation
2.0	Sample-1	– 10.53	– 23.12	11.32	16.56	1.84	5.08
	Sample-2	– 20.27	– 25.31	18.00	18.00	2.84	2.92
2.5	Sample-1	– 8.67	– 20.92	8.64	12.56	0	6.16
	Sample-2	– 19.88	– 24.84	14.80	14.24	6.24	6.40
3.0	Sample-1	– 7.92	– 25.95	6.80	10.36	0	4.68
	Sample-2	– 19.35	– 25.31	11.52	11.52	5.16	5.76